

Resolving Fermi, PAMELA and ATIC anomalies in split supersymmetry without R-parity

Chuan-Hung Chen^{1,2*}, Chao-Qiang Geng^{3†} and Dmitry V. Zhuridov^{3‡}

¹*Department of Physics, National Cheng-Kung University, Tainan 701, Taiwan*

²*National Center for Theoretical Sciences, Hsinchu 300, Taiwan*

³*Department of Physics, National Tsing-Hua University, Hsinchu, 300 Taiwan*

(Dated: May 30, 2019)

Abstract

A long-lived decaying dark matter as a resolution to Fermi, PAMELA and ATIC anomalies is investigated in the framework of split supersymmetry (SUSY) without R-parity, where the neutralino is regarded as the dark matter and the extreme fine-tuned couplings for the long-lived neutralino are naturally evaded in the usual approach. The energy spectra of electron and positron are from not only the direct neutralino decays denoted by $\chi \rightarrow e^+e^-\nu$, but also the decaying chains such as $\chi \rightarrow e^+\nu\mu(\rightarrow \nu_\mu e\bar{\nu}_e)$. We find that with a proper lifetime of the neutralino, slepton-mediated effects could explain the ATIC and PAMELA data well, but a inconsistency occurs to it the Fermi and PAMELA data without considering the ATIC one. Moreover, by a suitable combination of $\chi \rightarrow e^+e^-\nu$ and $\chi \rightarrow e^+\nu\mu(\rightarrow \nu_\mu e\bar{\nu}_e)$, the sneutrino-mediated effects could simultaneously account for the Fermi and PAMELA data.

* Email: physchen@mail.ncku.edu.tw

† Email: geng@phys.nthu.edu.tw

‡ Email: zhuridov@phys.nthu.edu.tw

It is mysterious that the direct measured matter in the standard model (SM) only occupies 4% of our universe while dark matter and dark energy have the occupancies of 22% and 74%, respectively. It becomes a very important issue to understand what the dark stuff is. Through the high energy collider such as Large Hadron Collider (LHC) at CERN, we may directly observe the dark matter. On the other hand, by the study of the high energy cosmic-ray, we may have the chance to probe the dark matter indirectly.

Recently, PAMELA [1] and ATIC [2] collaborations have published some astonished events in cosmic-ray measurements, in which the former finds the excess in the positron flux ratio with energies in the 10 – 100 GeV range, while the later observes anomaly in the electron+positron flux in the 300 – 800 GeV range. Intriguingly, these data are consistent with the measurements of the high energy electron and positron fluxes in the cosmic ray spectra by PPB-BETS [3], HEAT [4], AMS [5] and HESS [6], respectively. Inspired by the PAMELA/ATIC anomalies, various interesting possible mechanisms to generate the high energy positrons and electrons are proposed, such as pulsars [7], dark matter annihilations [8] and dark matter decays [9, 10]. Very recently, a more precision measurement on the electron+positron flux by the Fermi collaboration [11] with the similar energy range as ATIC has shown some enhancement in flux in the higher energy range. However, the Fermi's result indicates a smaller flux in the 500 GeV range. Nevertheless, in our study we consider both data. Other relevant studies could be referred to Ref. [12].

Although the mechanism of dark matter annihilations could provide the source for the Fermi, PAMELA and ATIC (FPA) anomalies, it is inevitable that an enhanced boost factor of a few orders of magnitude, such as Sommerfeld enhancement [13], near-threshold resonances and dark-onium formation [14], has to be introduced. In this paper, we investigate other sources for the excess of positrons and electrons in FPA without a large boost factor. We will concentrate on the mechanism of dark matter decays. As known that in order to make the unstable dark matter be long-lived, say $O(10^{26}s)$, usually we have to fine-tune either couplings to be tiny or the scale of the intermediate state to be as large as the GUT scale [10]. Therefore, our purpose is to explore what kind of long-lived dark matter in the extension of the SM that could satisfy one of two criteria naturally, at least in technique.

In the literature, one of the popular SM extensions is supersymmetry (SUSY). It has been known that the effects of SUSY at the scale Λ of $O(\text{TeV})$ can solve not only the hierarchy problem, but also the problem of the unified gauge coupling [15, 16]. Moreover, the predicted

lightest neutralino in supersymmetric models could also provide the candidate of dark matter [15, 17]. In spite of the above successes, models with SUSY still suffer some difficulties from phenomenological reasons, such as the problems on small CP violating phases, large flavor mixings and proton decays, as well as they predict too large cosmological constant. As a result, inevitably, a fine tuning always comes up in the low energy physics. In order to interpret the cosmological constant problem and maintain the beauty of the ordinary low-energy SUSY models, the scenario of split SUSY is suggested [18, 19], in which the SUSY breaking scale is much higher than the electroweak scale. In this split SUSY scenario, except the SM Higgs which could be as light as the current experimental limit, the scalar particles are all ultra-heavy, denoted by $m_S \sim \mathcal{O}(> 10^9)$ GeV. On the other hand, by the protection of approximate chiral symmetries, the masses of sfermions, such as gauginos and higgsinos, could be at the electroweak scale [18, 20]. Clearly, split SUSY not only supplies the candidate of fermionic dark matter at the TeV scale but also provides a large scale for the SUSY breaking, so that the second criterion mentioned early for model-searches is satisfied automatically. Thus, if the ultraheavy scalar sparticles could play the role of messenger to deliver the dark matter decay, the decaying rate of the dark stuff is suppressed and the lifetime of unstable dark matter could be still long enough to explain the FPA puzzle.

In split supersymmetric models with R-parity, the neutralino regarded as the lightest SUSY particle (LSP) is stable particle. To study the dark matter decays, we extend our consideration to the framework of split SUSY with the violation of R-parity, in which the conservations of lepton or/and baryon numbers are broken. Since FPA anomalies only involve leptons, it is plausible to only consider lepton number violating effects by requiring a good symmetry on the baryon number. As usual, the superpotential for the minimal supersymmetric standard model (MSSM) with bilinear and trilinear terms that violate the lepton number violation is expressed by

$$\begin{aligned}
W &= W_{\text{MSSM}} + W_{\mathcal{R}}, \\
W_{\text{MSSM}} &= h_{ij}^{\ell} L_i H_d E_j^c + h_{ij}^d Q_i H_d D_j^c + h_{ij}^u Q_i H_u U_j^c + \mu H_d H_u, \\
W_{\mathcal{R}} &= \frac{1}{2} \lambda_{[ij]k} L_i L_j E_k^c + \lambda'_{ijk} L_i Q_j D_k^c + \epsilon_i L_i H_u.
\end{aligned} \tag{1}$$

We note that the bilinear term $L_i H_u$ could be rotated away by redefining the superfield as $H_d \rightarrow (\mu^2 + \epsilon_i \epsilon_j)^{-1/2} (\mu H_d - \epsilon_i L_i)$. In the ordinary SUSY model, the bilinear operator could be reinduced by loop effects. However, in the scenario of split SUSY, since all bosonic

sparticles are very heavy, the loop induced effects are highly suppressed and negligible [21]. In addition, with the measurement on the antiproton flux by PAMELA that shows no exotic events, it is conceivable to set the quarks related effects governed by the parameters λ'_{ijk} as small as possible. Thus, in our analysis, we will only focus on trilinear interactions of $W_R = 1/2\lambda_{[ij]k}L_iL_jE_k^c$. Consequently, the Lagrangian for the R-parity violation is found to be

$$\begin{aligned}\mathcal{L}_R = & \lambda_{[ij]k} \left(\bar{\ell}_k P_L \ell_j \tilde{\nu}_{iL} + \bar{\ell}_k P_L \nu_{iL} \tilde{\ell}_{jL} + \bar{\ell}_j P_R \nu_{iL}^c \tilde{\ell}_{kR} \right. \\ & \left. - \bar{\ell}_k P_L \ell_i \tilde{\nu}_{jL} - \bar{\ell}_k P_L \nu_{jL} \tilde{\ell}_{iL} - \bar{\ell}_i P_R \nu_{jL}^c \tilde{\ell}_{kR} \right) + \text{H.c.}\end{aligned}\quad (2)$$

with $P_{R(L)} = (1 \pm \gamma_5)/2$. The bracket [ij] denotes that the λ parameters are antisymmetry in the first two indices. Since in MSSM neutralinos are composed of bino, wino and higgsinos, for simplicity, we take the bino as the neutralino denoted by $\tilde{\chi}_1^0$ and the couplings to leptons are given by [22]

$$\mathcal{L}_{\tilde{\chi}_1^0 \ell \tilde{\ell}} = \frac{g}{\sqrt{2}} \tan \theta_W \bar{\ell} \left[c_L^\ell P_R \tilde{\ell}_L + c_R^\ell P_L \tilde{\ell}_R \right] \tilde{\chi}_1^0 \quad (3)$$

with θ_W being Weinberg angle, $c_R^\ell = -2$ and $c_L^\ell = 1$ for charged leptons and $c_L^\nu = 1$ for neutrinos.

According to Eqs. (2) and (3), we see that split SUSY with the R-parity violation has two channels to decay to the charged leptons: one is via the charged sleptons and another one is mediated by sneutrinos, where we sketch the Feynman diagrams in Fig. 1. Before we make the detailed analysis for the energy spectra of electron and positron in neutralino decays, it is worthwhile to understand the allowed range of free parameters to satisfy the condition of long-lived dark matter. Since there are 6 (3) species of sleptons (sneutrinos) and many free parameters in $\lambda_{[ij]k}$, to simplify the estimation and without loss of generality, we use one single decaying channel, associated with slepton as the mediator, to illustrate what the lifetime of the neutralino could be. Thus, based on the introduced interactions, we obtain the lifetime of the neutralino to be

$$\tau_\chi \simeq \frac{3\sqrt{2}2^9\pi^3}{G_F m_W^2 \tan^2 \theta_W} \frac{m_{\tilde{\ell}}^4}{|\lambda_{[ij]k}|^2 m_\chi^5}. \quad (4)$$

With $m_\chi = 2$ TeV, the lifetime as a function of the slepton mass and trilinear coupling is shown in Fig. 2. In the figure, we have used λ instead of $\lambda_{[ij]k}$. The typical values of τ_χ are chosen according to the necessity to fit the data of FPA. Clearly, in split SUSY, with the

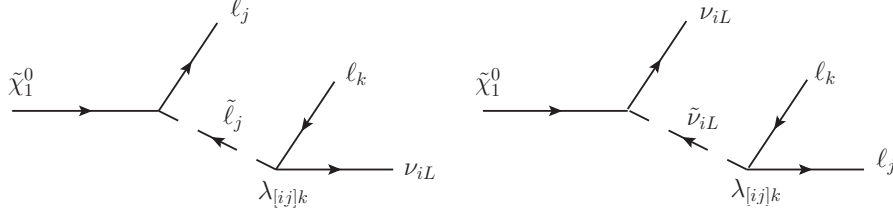


FIG. 1: The Feynman diagram for LSP decay in split SUSY.

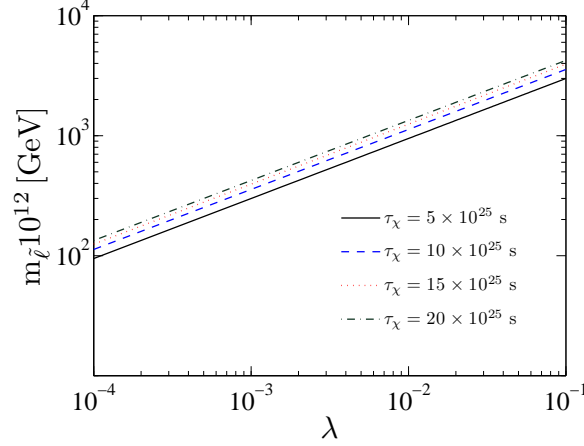


FIG. 2: Typical lifetime for PAMELA/ATIC anomalies as a function of the slepton mass and the unspecified parameter $\lambda = \lambda_{[ij]k}$ in log scale.

SUSY breaking scale of $m_{\tilde{\ell}} \sim O(10^{13} - 10^{15})$ GeV and $\lambda \sim O(10^{-4} - 10^{-1})$, τ_χ could be much longer than the age of our universe with $O(10^{17})$ s.

Since multi-indices are involved in $\lambda_{[ij]k}$, there are many possible channels to produce the high energy positrons and electrons. In order to display the characters of neutralino decays in split SUSY efficiently, we will study the cases in which the final states involve an electron-positron pair or one electron (positron) associated with one anti-muon (muon). For the latter case, anti-muon (muon) will further decay to positron (electron) due to weak interactions of the SM. In short, we will focus on the decays $\tilde{\chi}_1^0 \rightarrow e^\pm \nu_{iL} e^\mp$ and $\tilde{\chi}_1^0 \rightarrow e^\pm \nu_{iL} \mu^\mp (\rightarrow \nu_\mu e^\mp \nu_e)$, where the relevant R-parity violating couplings are $\lambda_{[i1]1}$, $\lambda_{[i1]2}$ and $\lambda_{[i2]1}$. In addition, since for each flavor of slepton, we have two sparticles $\tilde{\ell}_L$ and $\tilde{\ell}_R$ that correspond to the superpartners of left-handed and right-handed leptons, respectively, in weak states. For simplicity, in our following analysis, we will concentrate on the contributions of $\tilde{\ell}_L$. Expectably, the effects of $\tilde{\ell}_R$ on the energy spectra of electron and positron should be

very similar to those of $\tilde{\ell}_L$.

According to our setup on the conditions for split SUSY without R-parity, the corresponding Feynman diagrams are displayed in Fig. 3. Since Figs. 3(a) and (b) are mediated by the selectron while Figs. 3 (c) and (d) are exchanged by the sneutrino, we separately study the energy spectrum of electron induced by these diagrams. Moreover, to be more

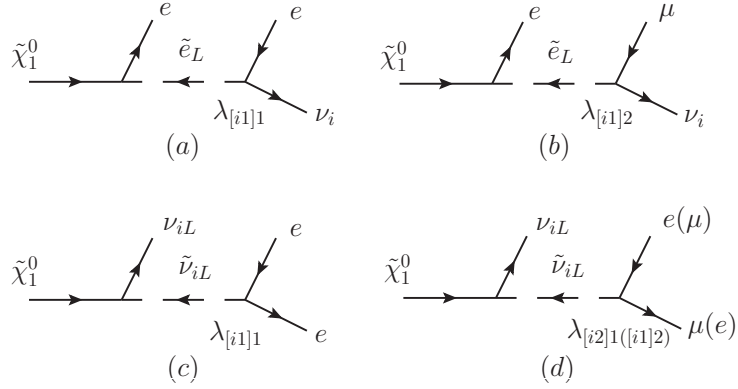


FIG. 3: Feynman diagrams for the neutralino decays in split SUSY.

clear, we discuss the contributions in terms of the individual diagram in Fig. 3. Following the interactions in Eqs. (2) and (3), the decay amplitude for Fig. 3(a) can be written as

$$M_a = i \frac{g}{\sqrt{2}} c_L^e \tan \theta_W \frac{\lambda_{[i1]1}}{m_{\tilde{e}_L}^2} \bar{u}_e P_R \tilde{\chi}_1^0 \tilde{\nu}_{iL} P_R v_e, \quad (5)$$

where $u_e(v_e)$ denotes the Dirac spinor of electron (positron). We note that since the emitted lepton from the first vertex connected to the neutralino is electron or positron, Eq. (5) could be also applied to the case where the electron is emitted at the second vertex associated with the neutrino. By combining both possibilities and including the phase space for the three-body decay, the differential rate as a function of the electron energy is obtained to be

$$\begin{aligned} \frac{d\Gamma_a}{dE} &= \frac{C_\chi}{3} |\lambda_{[i1]1}|^2 E^2 (9m_\chi^2 - 16m_\chi E), \\ C_\chi &= \frac{|c_L^e \tan \theta_W|^2}{2^5 \sqrt{2} \pi^3} \frac{G_F m_W^2}{m_{\tilde{e}_L}^2}. \end{aligned} \quad (6)$$

The allowed range of E is known as $0 \leq E \leq m_\chi/2$. This energy spectrum should be also suitable for positron. Accordingly, the normalized spectrum is defined by

$$\frac{dN_a}{dE} = \frac{d\Gamma_a/dE}{\int_0^{E^{\max}} dE d\Gamma_a/dE} \quad (7)$$

with $E^{\max} = m_\chi/2$. For Fig. 3(b), due to muon involved, the situation is a little bit complicated. According to the previous analysis, the spectrum for electron directly emitted from the neutralino decay can be easily read by

$$\frac{d\Gamma_{b1}}{dE} = 2C_\chi |\lambda_{[i1]2}|^2 E^2 (m_\chi^2 - 2m_\chi E). \quad (8)$$

However, if the electron is produced via the muon decay, we have to deal with the decaying chain, i.e. $\tilde{\chi}_1^0 \rightarrow e^+ \nu_{iL} \mu^- (\rightarrow \nu_\mu e^- \bar{\nu}_e)$. We find that indeed the differential decay rate for the decaying chain can be simplified to be

$$d^2\Gamma_{b2} = d\Gamma_\mu^{\tilde{\ell}} \frac{1}{2m_\mu \Gamma_\mu} \frac{d|M_\mu|^2}{2} \quad (9)$$

where $d\Gamma_\mu^{\tilde{\ell}}$ denotes the decay rate for $\tilde{\chi}_1^0 \rightarrow e^+ \mu^- \nu_{iL}$, $d|M_\mu|^2$ has combined the amplitude square for $\mu^- \rightarrow \nu_\mu e \bar{\nu}_e$ and the three-body phase space and Γ_μ is the total width of muon. If we further integrate out all the angles, we get

$$\begin{aligned} d\Gamma_\mu^{\tilde{\ell}}(E_\mu) &= C_\chi |\lambda_{[i1]2}|^2 E_\mu^2 \left(m_\chi^2 - \frac{4}{3} m_\chi E_\mu \right) dE_\mu, \\ d|M_\mu|^2(E_\mu, E) &= \frac{G_F^2}{6\pi^3} \frac{1}{|\vec{p}_\mu|} \left\{ \frac{4}{3} \left[E^3 (E_\mu - |\vec{p}_\mu|)^3 - \left(\frac{m_\mu^2}{2} \right)^3 \right] \right. \\ &\quad \left. - \frac{3}{2} m_\mu^2 \left[E^2 (E_\mu - |\vec{p}_\mu|)^2 - \left(\frac{m_\mu^2}{2} \right)^2 \right] \right\} dE. \end{aligned} \quad (10)$$

Here, the allowed energy range for muon and electron are found to be $m_\mu \leq E_\mu \leq m_\chi/2$ and $0 \leq E \leq m_\mu^2/2(E_\mu - |\vec{p}_\mu|)$, respectively. From the analysis, we know that in the rest frame of muon, the upper value of E is $m_\mu/2$, however, for energetic muon, the upper value becomes E_μ . We adopt the normalized energy spectrum of electron (positron) for Fig. 3(b) to be

$$\frac{dN_b}{dE} = \frac{d\Gamma_{b1}/dE + \int_{m_\mu}^{E_\mu^{\max}} dE_\mu d^2\Gamma_{b2}/dE/dE_\mu}{\int_0^{E^{\max}} dE \left[d\Gamma_{b1}/dE + \int_{m_\mu}^{E_\mu^{\max}} dE_\mu (d^2\Gamma_{b2}/dE/dE_\mu) \right]}. \quad (11)$$

Similarly, we can apply the calculations for slepton-mediated effects to Figs. 3(c) and (d) mediated by sneutrinos. Utilizing the results in Eq. (10) by replacing suitable coefficients and parameters, the differential decay rate for Fig. 3(c) is easily obtained as

$$\frac{d\Gamma_c(E)}{dE} = C_\chi \left| \frac{c_L^\nu}{c_L^\ell} \frac{m_{\tilde{\ell}_L}^2}{m_{\tilde{\nu}_L}^2} \right|^2 |\lambda_{[i1]1}|^2 E^2 \left(m_\chi^2 - \frac{4}{3} m_\chi E \right). \quad (12)$$

Following the definition of Eq. (7), we can get the normalized energy spectrum for Fig. 3(c). Since Fig. 3(d) involves muon in the final state, similar to figure (b), we have to deal with the decaying chain such as $\tilde{\chi}_1^0 \rightarrow \nu_{iL} e^+ \mu^- (\rightarrow \nu_\mu e \bar{\nu}_e)$. By comparing with Eq. (9), the differential decay rate for the decaying chain is given by

$$d^2\Gamma_d = d\Gamma_\mu^{\tilde{\nu}} \frac{1}{2m_\mu\Gamma_\mu} \frac{d|M_\mu|^2}{2} \quad (13)$$

with

$$d\Gamma_\mu^{\tilde{\nu}} = \frac{|\lambda_{[i2]1}|^2 + |\lambda_{[i1]2}|^2}{|\lambda_{[i1]1}|^2} d\Gamma_c(E_\mu). \quad (14)$$

The corresponding normalized spectrum is

$$\frac{dN_d}{dE} = \frac{\int_{m_\mu}^{E_{\max}} dE_\mu d^2\Gamma_d/dE/dE_\mu}{\int_0^{E_{\max}} dE \left[d \int_{m_\mu}^{E_{\max}} dE_\mu (d^2\Gamma_d/dE/dE_\mu) \right]}. \quad (15)$$

To study the measured cosmic-ray, we have to know the behavior of the number density of particles per unit energy, governed by the transport equation [23, 24]

$$\frac{\partial f}{\partial t} = \nabla \cdot (K(E, \vec{r}) \nabla f) + \frac{\partial}{\partial E} (b(E, \vec{r}) f) + Q_e(E, \vec{r}), \quad (16)$$

where $f(E, \vec{r})$ denotes the number density of cosmic-ray per unit energy, $K(E, \vec{r})$ is the diffusion coefficient, $b(E, \vec{r})$ describes the rate of the energy loss by the inverse Compton scattering and synchrotron radiation etc., and $Q(E, \vec{r})$ represents the source of cosmic-ray from the decay of dark matter, given by

$$Q(E, \vec{r}) = \frac{\rho_\chi(\vec{r})}{m_\chi \tau_\chi} \frac{dN}{dE}, \quad (17)$$

with τ_χ (m_χ) the lifetime (mass) of dark matter, dN/dE the energy spectrum of cosmic-ray and $\rho_\chi(\vec{r})$ the density profile of dark matter. In our following analysis, we will adopt the so-called Navarro-Frenk-White (NFW) profile, given by [25]

$$\rho_\chi = \frac{\rho_0 r_c^3}{r(r_c + r)^2} \quad (18)$$

with $\rho_0 = 0.26 \text{ GeV/cm}^3$ and $r_c = 20 \text{ kpc}$. By using the Green function method, the steady solution to Eq. (16) for electron and positron can be expressed by

$$f(E) = \frac{1}{m_\chi \tau_\chi} \int_0^{m_\chi/2} dE' G(E, E') \frac{dN}{dE'}. \quad (19)$$

Since the experiments measure the flux of cosmic-rays, the relation to the number density is given by $\Phi^\chi = cf(E)/(4\pi)$ with c being the speed of light. For numerical estimations, we adopt the result parametrized by [24]

$$G(E, E') \simeq \frac{10^{16}}{E^2} \exp[a + b(E^{\delta-1} - E'^{\delta-1})]\theta(E' - E) \quad [\text{cm}^{-3}\text{s}] \quad (20)$$

with $a = -1.0203$, $b = -1.4493$ and $\delta = 0.70$. We note that these values of parameters should depend on the modeling for the profile of dark matter in our Galaxy. The detailed analysis on the dependence of various profiles can be referred to Ref. [24].

Besides the new source for the fluxes of electron and positron, we also need to understand the contributions of primary and secondary electrons and secondary positrons, in which the former comes from supernova remnants and the spallation of cosmic rays in the interstellar medium, respectively, while the latter could be generated by primary protons colliding with other nuclei in the interstellar medium. In our numerical calculations, we use the parametrizations, given by [26, 27]

$$\begin{aligned} \Phi_{e^-}^{\text{prim}}(E) &= \frac{0.16E^{-1.1}}{1 + 11E^{0.9} + 3.2E^{2.15}} \quad [\text{GeV}^{-1}\text{cm}^{-2}\text{s}^{-1}\text{sr}^{-1}], \\ \Phi_{e^-}^{\text{sec}}(E) &= \frac{0.7E^{0.7}}{1 + 110E^{1.5} + 600E^{2.9} + 580E^{4.2}} \quad [\text{GeV}^{-1}\text{cm}^{-2}\text{s}^{-1}\text{sr}^{-1}], \\ \Phi_{e^+}^{\text{sec}}(E) &= \frac{4.5E^{0.7}}{1 + 650E^{2.3} + 1500E^{4.2}} \quad [\text{GeV}^{-1}\text{cm}^{-2}\text{s}^{-1}\text{sr}^{-1}] \end{aligned} \quad (21)$$

where $\Phi^{\text{prim(sec)}}$ denotes the primary (secondary) cosmic ray. Accordingly, the total electron and positron fluxes are defined by

$$\begin{aligned} \Phi_{e^-} &= \kappa\Phi_{e^-}^{\text{prim}} + \Phi_{e^-}^{\text{sec}} + \Phi_{e^-}^\chi, \\ \Phi_{e^+} &= \Phi_{e^+}^{\text{sec}} + \Phi_{e^+}^\chi. \end{aligned} \quad (22)$$

Here, according to Refs. [27] and [28], we have regarded the normalization of the primary electron flux to be undetermined and parametrized by the parameter of κ . The value of κ is chosen to fit the data. Before introducing the source of the primary positron, κ is set to be 0.8. For comparison, we show the background with $\kappa = 0.8$ and current data as a function of the cosmic-ray energy in Fig. 4.

Now we start to numerically analyze the influence of long-lived neutralino decays on the electron and positron fluxes in split SUSY. To fit the PAMELA and ATIC (Fermi) data, we take

$$\tau_\chi = 2 \times 10^{26} (4 \times 10^{26}) \text{s}, \quad m_\chi = 2 \text{ TeV}, \quad \kappa = 0.7, \quad (23)$$

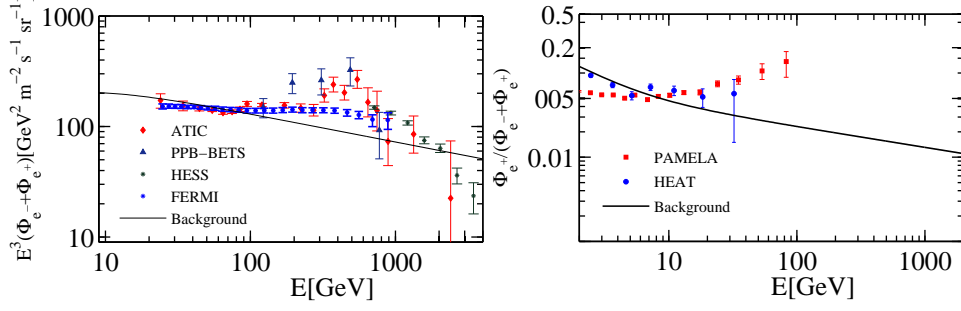


FIG. 4: Various current data for fluxes of positron and electron as a function of the cosmic-ray energy. The background is based on Eqs. (21) and (22) with $\kappa = 0.8$.

respectively. Since Fermi and ATIC both show the electron+positron flux, we will make detailed discussions in the light of the ATIC's measurement and extend the analysis to include Fermi accordingly. Based on our earlier discussions, we also present our numerical results by diagrams shown in Fig. 3. Hence, in terms of Eqs. (7), (21) and (22), the contributions of Fig. 3(a) are displayed in Fig. 5(a), where the left-hand side is for the electron + positron flux while the right-hand side is the ratio of the positron flux to electron+positron flux. The thin line stands for the background with $\kappa = 0.8$ before including the split SUSY effects. The thick solid (dashed) line denotes the result with (without) the background. Since the PAMELA data show the ratio of fluxes, it should be a constant line with unity if we turn off the contributions of the background. Thus, for PAMELA, we only show the results associated with the background. From our results, it is clear that the energy spectrum of Fig. 3(a) shown in Eq. (7) matches the PAMELA and ATIC data up to 1 TeV well. It is worthy to mention that since we only consider one channel for Fig. 3(a) with the normalization of Eq. (7), the energy spectra of cosmic rays have no dependences on the slepton mass and the couplings given in Eqs. (2) and (3). The same situation will appear in the analysis on the other individual diagram. However, the parameters will be involved when we consider different diagrams together. We will see this point more clear later.

For the effects of Fig. 3(b), where electron and positron can be emitted directly from neutralino and muon decays, we show their contributions in Fig. 5(b). Here, the dashed and dash-dotted lines correspond to Eq. (8) and Eq. (9) without the background, respectively. The thick solid lines on left and right-hand sides are the combined effects with the background. From the figure, we see clearly that below 300 GeV, the spectrum from one

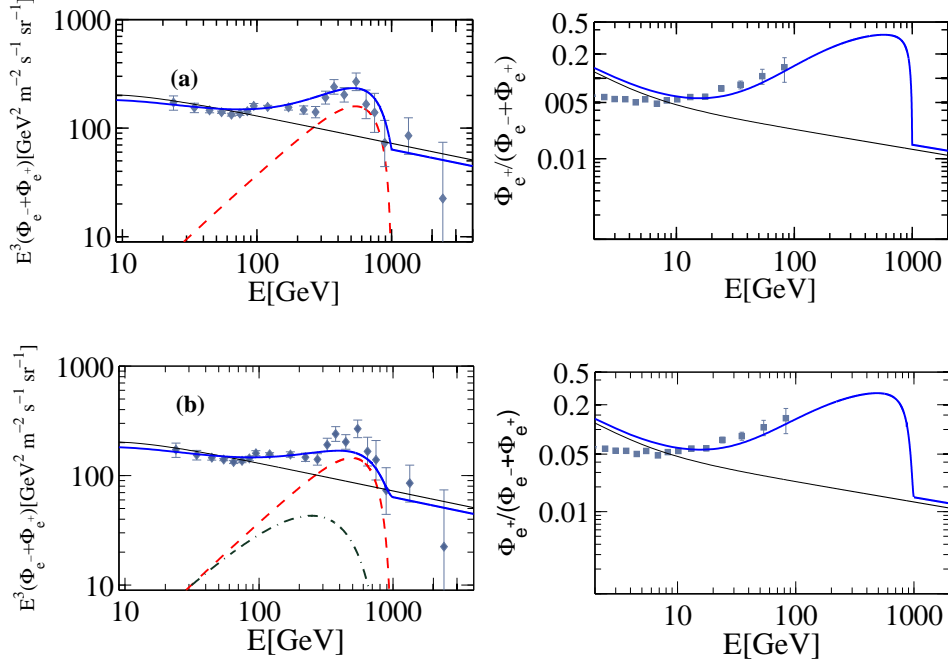


FIG. 5: (a) [(b)] The effects of Fig. 3(a) [(b)] on the ATIC and PAMELA anomalies, where the thin solid line is the background with $\kappa = 0.8$, the thick solid (dashed, dash-dotted) line for ATIC denotes the effect with (without) the background, and the dashed and dash-dotted lines in (b) represent the contribution of $d\Gamma_{b1}/dE$ and $d\Gamma_{b2}/dE$, respectively.

electron and one muon ($e + \mu$) in neutralino decay fits the ATIC data well, but it is lower at the higher energy. Nevertheless, the $e + \mu$ mechanism still matches well with the PAMELA data. After the discussions of the individual contributions from Figs. 3(a) and (b), it is

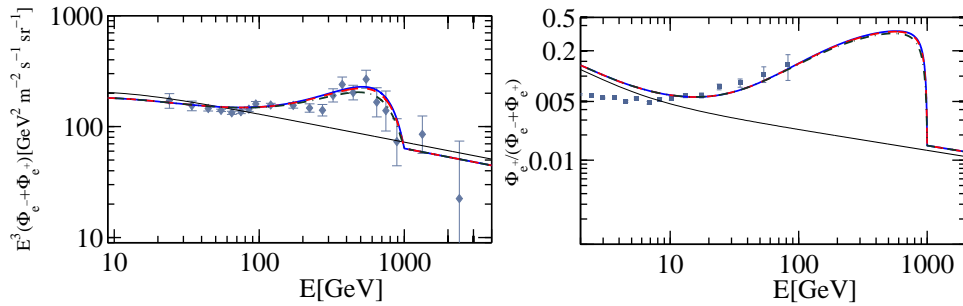


FIG. 6: The results by combining Fig. 3(a) and (b) with different partitions described by (c_ζ^2, s_ζ^2) , where the solid, dashed and dash-dotted lines stand for $(0.8, 0.2)$, $(0.6, 0.4)$ and $(0.3, 0.7)$, respectively.

interesting to consider their combination effects. Due to both mechanisms being mediated

by the selectron, the energy spectrum now will depend on the free parameters $\lambda_{[i1]1}$ and $\lambda_{[i1]2}$. In order to simplify the analysis, we use new parameter ζ that satisfies $c_\zeta^2 + s_\zeta^2 = 1$ instead of the original ones which appear with the form of $|\lambda_{[i1]1(2)}|^2$ in Eqs. (6) and (10). Therefore, the new normalized energy spectrum for electron (positron) is given by

$$\frac{dN_{a+b}}{dE} = \frac{c_\zeta^2 dZ_a/dE + s_\zeta^2 dZ_b/dE}{\int_0^{E^{\max}} dE (c_\zeta^2 dZ_a/dE + s_\zeta^2 dZ_b/dE)} \quad (24)$$

with

$$\begin{aligned} \frac{dZ_a}{dE} &= \frac{1}{|\lambda_{[i1]1}|^2} \frac{d\Gamma_a}{dE}, \\ \frac{dZ_b}{dE} &= \frac{1}{|\lambda_{[i1]2}|^2} \left(\frac{d\Gamma_{b1}}{dE} + \int_{m_\mu}^{E_\mu^{\max}} dE_\mu \frac{d^2\Gamma_{b2}}{dE dE_\mu} \right). \end{aligned} \quad (25)$$

Consequently, by combining Eq. (24) with Eqs. (21) and (22), the results are shown in Fig. 6 where the solid, dashed and dash-dotted lines correspond to the cases of $(c_\zeta^2, s_\zeta^2) = (0.8, 0.2)$, $(0.6, 0.4)$ and $(0.3, 0.7)$, respectively. By the figure, we see that the spectrum mediated by the selectron through the mechanisms of Figs. 3(a) and (b) is not sensitive to the detailed partition for the percentage of $\lambda_{[i1]1}$ and $\lambda_{[i1]2}$. Intriguingly, the resultant combination is consistent with the PAMELA and ATIC data.

As shown before, the flux measured by Fermi is more precise and smaller than that by ATIC at the high energy region. Since all involved parameters for ATIC and Fermi are the same, to singly fit the Fermi data, we only need to tune the lifetime of the neutralino. Therefore, with $\tau_\chi = 4 \times 10^{26}$ s, the combination effects of Figs. 3(a) and (b) are presented in Fig. ???. It is clear to see that we can fit the Fermi data in split SUSY. However, the

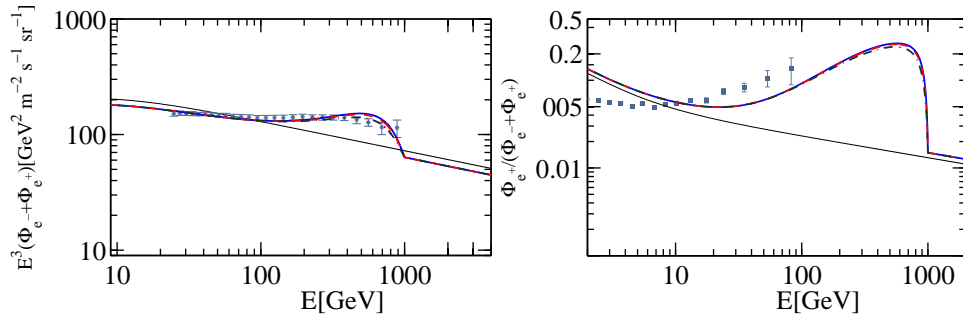


FIG. 7: The legend is the same as Fig. 6 but with $\tau_\chi = 4 \times 10^{26}$ s.

result for the positron flux ratio deviates from the PAMELA's results.

Next, we study the sneutrino-mediated effects shown in Fig. 3(c) and (d). Since electron or positron can not be emitted from the vertex of the decaying neutralino in this case, the electron-positron pair or electron-antimuon (positron-muon) final state is only produced via the R-parity violating interactions. Therefore, the resultant cosmic-ray fluxes may differ from the processes mediated by the selectron. With Eq. (12) and the normalization defined in Eq. (7), we show the electron+positron flux and the ratio of the positron flux in Fig. 8(c), where the solid (dashed) line is associated with (without) the background. Clearly, the result of the mechanism not only roughly fit the ATIC's data but also explain the PAMELA's measurement well. By the analysis, we see that the energy spectra governed by $E^2(9m_\chi^2 - 16m_\xi E)$ of Eq. (6) and $E^2(m_\chi^2 - 4/3m_\chi E)$ of Eq. (12) have similar results.

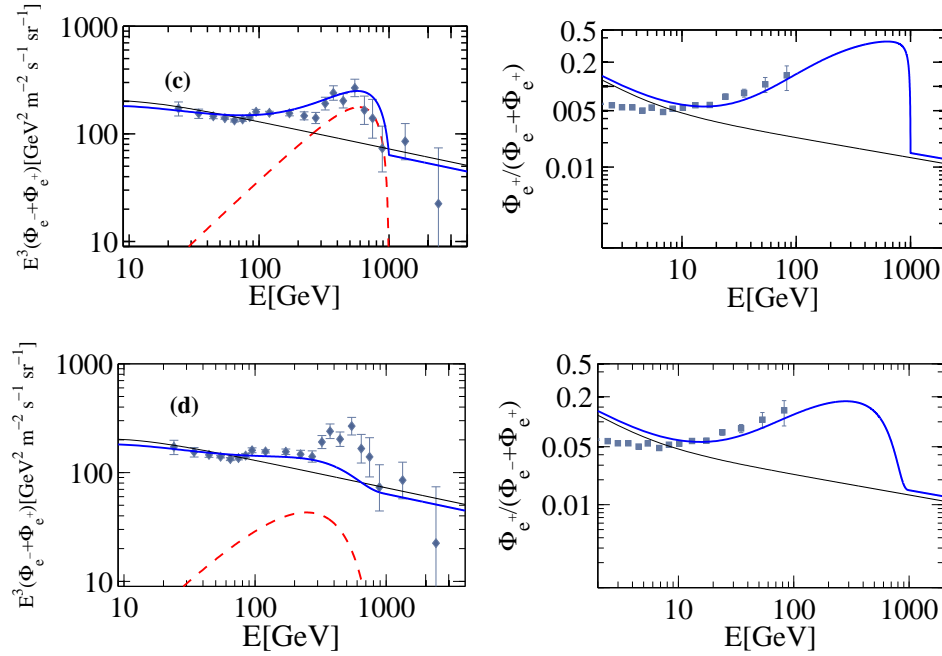


FIG. 8: (c) [(d)] Results explain the ATIC and PAMELA anomalies by Fig. 3(c) [(d)], where the solid (dashed) line for ATIC denotes the effect with (without) the background.

As to the contributions of one electron (positron) and one anti-muon (muon) formulated by Eq. (15), we present the results in Fig. 8(d). We note that Eq. (15) involves two free parameters of $\lambda_{[i1]2}$ and $\lambda_{[i2]1}$. For simplicity, we have set $\lambda_{[i1]2} = \lambda_{[i2]1}$. Similar to the $e + \mu$ mechanism of Fig. 3(b), it could also match the PAMELA data well. Although the shapes of fluxes in Figs. 5(b) and 8(d) look similar, the decreasing tendency at the high energy in the latter is faster than that in the former. Moreover, in Fig. 9 we display the

combination of Figs. 8(c) and (d), where we have followed the approach used in Eq. (24) to introduce a new parameter c_ζ^2 (s_ζ^2) instead of the old parameters of $\lambda_{[i1]1}$ and $\lambda_{[i1(2)]2(1)}$. The solid, dashed and dash-dotted lines in the figure denote $(c_\zeta^2, s_\zeta^2) = (0.8, 0.2)$, $(0.6, 0.4)$ and $(0.3, 0.7)$, respectively. It is clear that the resultant fluxes mediated by sneutrino at

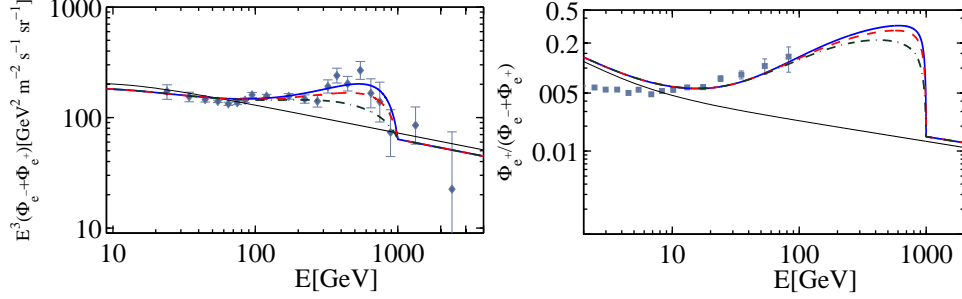


FIG. 9: Legend is the same as Fig. 6, but for Fig. 3(c) and (d).

the energy above 200 GeV are sensitive to the percentage of dN_c/dE and dN_d/dE . When the percentage of dN_c/dE (dN_d/dE) decreases (increases), the positron+electron flux is also decreased accordingly. Intuitively, the resultant shape of the flux is very close to what Fermi observes. If we directly use the result in Fig. 9 to compare with the Fermi data shown in Fig. 10, we find that the result with $(c_\zeta^2, s_\zeta^2) = (0.3, 0.7)$ could fit the Fermi data very

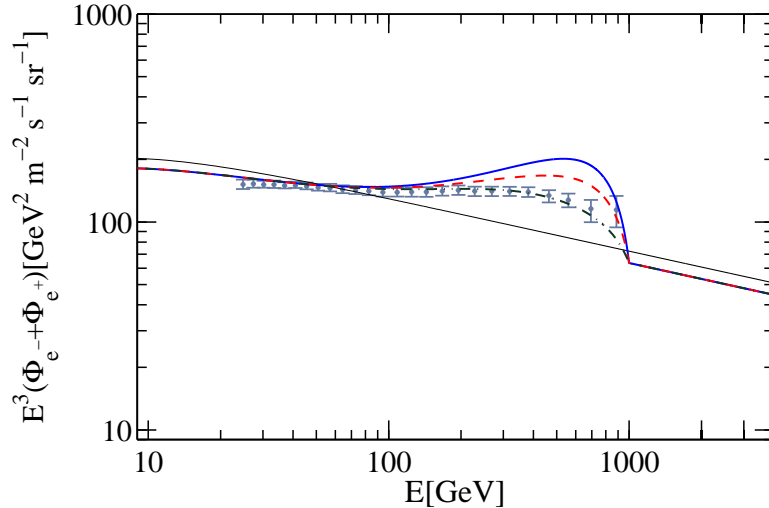


FIG. 10: The positron+electron flux from Figs. 3 (c) and (d) due to the sneutrino.

well. Importantly, unlike the slepton-mediated case, with the same parameters, Fermi and PAMELA anomalies can be understood simultaneously.

In summary, we have investigated the Fermi, PAMELA and ATIC anomalies in the framework of split SUSY without R-parity based on the neutralino decays. We have shown that the energy spectra of electron and positron are from not only the direct neutralino decays denoted by $\chi \rightarrow e^+e^-\nu$, but also the decaying chains such as $\chi \rightarrow e^+\nu\mu(\rightarrow \nu_\mu e\bar{\nu}_e)$. We have studied both types of channels separately and unitedly in detail. We have found that with $\tau_\chi = 2 \times 10^{26}$ s, slepton-mediated effects could explain the ATIC and PAMELA data well but not for the Fermi and PAMELA data even with a different neutralino lifetime. However, by the proper combination of $\chi \rightarrow e^+e^-\nu$ and $\chi \rightarrow e^+\nu\mu(\rightarrow \nu_\mu e\bar{\nu}_e)$, the sneutrino-mediated effects could fit the Fermi and PAMELA data simultaneously.

Acknowledgements

We would like to thank Prof. Shih-Chang Lee and Prof. Tsz-King Wong for useful discussions. This work is supported in part by the National Science Council of R.O.C. under Grant Nos: NSC- 97-2112-M-006-001-MY3 and NSC-95-2112-M-007-059-MY3.

-
- [1] O. Adriani *et al.* [PAMELA Collaboration], Nature **458**, 607 (2009). [arXiv:0810.4995 [astro-ph]].
 - [2] J. Chang *et al.* [ATIC Collaboration], Nature **456**, 362 (2008).
 - [3] S. Torii *et al.* [PPB-BETS Collaboration], arXiv:0809.0760 [astro-ph].
 - [4] S. W. Barwick *et al.* [HEAT Collaboration], Astrophys. J. **482**, L191 (1997).
 - [5] M. Aguilar *et al.* [AMS-01 Collaboration], Phys. Lett. B**646**, 145 (2007).
 - [6] F. Aharonian *et al.* [H.E.S.S. Collaboration], Phys. Rev. Lett. **101**, 261104 (2008) [arXiv:0811.3894[astro-ph]].
 - [7] D. Hooper, P. Blasi and P. D. Serpico, JCAP **0901**, 025 (2009) [arXiv:0810.1527]; H. Yuksel, M. D. Kistler and T. Stanev, arXiv:0810.2784 [astro-ph]; D. Malyshev, I. Cholis and J. Gelfand, arXiv:0903.1310 [astro-ph]; V. Barger *et al.*, arXiv:0904.2001 [hep-ph].
 - [8] L. Bergstrom, T. Bringmann and J. Edsjo, Phys. Rev. D**77**, 103520 (2008); M. Cirelli *et al.*, arXiv:0808.3867 [astro-ph]; 0809.2409 [hep-ph]; V. Barger *et al.*, Phys. Lett. B**672**,141 (2009); K. Cheung, P. Y. Tseng and T. C. Yuan, arXiv:0902.4035 [hep-ph]; D. S. M. Alves *et al.*,

- arXiv:0903.3945 [hep-ph].
- [9] C. R. Chen, F. Takahashi and T. T. Yanagida, Phys. Lett. **B671**, 71 (2009); Phys. Lett. **B673**, 255 (2009); C. R. Chen and F. Takahashi, JCAP **0902**, 004 (2009); P. F. Yin *et al.*, Phys. Rev. D **79**, 023512 (2009); K. Hamaguchi, E. Nakamura, S. Shirai, T. T. Yanagida, arXiv:0811.0737 [hep-ph]; A. Ibarra and D. Tran, JCAP **0902**, 021 (2009) [arXiv:0811.1555 [hep-ph]]; C. R. Chen, M. M. Nojiri, F. Takahashi and T. T. Yanagida, arXiv:0811.3357 [astro-ph]; E. Nardi, F. Sannino and A. Strumia, JCAP **0901**, 043 (2009) [arXiv:0811.4153 [hep-ph]]; A. Arvanitaki *et al.*, arXiv:0812.2075 [hep-ph]; K. Hamaguchi, S. Shirai and T. Yanagida, Phys. Lett. **B673**, 247 (2009) [arXiv:0812.2374 [hep-ph]]; K. Hamaguchi, F. Takahashi and T. T. Yanagida, arXiv:0901.2168 [hep-ph]; K. Ishiwata, S. Matsumoto and T. Moroi, arXiv:0903.0242 [hep-ph]; S. L. Chen *et al.*, arXiv:0903.2562 [hep-ph].
 - [10] C. H. Chen, C. Q. Geng and D. Zhuridov, Phys. Lett. **B675**, 77 (2009) [arXiv:0901.2681 [hep-ph]].
 - [11] A. A. Abdo *et al.* [Fermi LAT Collaboration], arXiv:0905.0025 [astro-ph.HE].
 - [12] L. Bergstrom, J. Edsjo and G. Zaharijas, arXiv:0905.0333 [astro-ph.HE]; S. Shirai, F. Takahashi and T. T. Yanagida, arXiv:0905.0388 [hep-ph].
 - [13] J. Hisano, S. Matsumoto and M. M. Nojiri, Phys. Rev. Lett. **92**, 031303 (2004) [arXiv:hep-ph/0307216]; N. Arkani-Hamed *et al.*, Phys. Rev. D **79**, 015014 (2009) [arXiv:0810.0713 [hep-ph]].
 - [14] M. Pospelov and A. Ritz, Phys. Rev. D **78**, 055003 (2008) [arXiv:0803.2251 [hep-ph]]; J. D. March-Russell and S. M. West, arXiv:0812.0559 [astro-ph].
 - [15] S. Dimopoulos and H. Georgi, Nucl. Phys. **B193**, 150 (1981).
 - [16] S. Dimopoulos, S. Raby and F. Wilczek, Phys. Rev. D **24**, 1681 (1981).
 - [17] H. Goldberg, Phys. Rev. Lett. **50**, 1419 (1983).
 - [18] N. Arkani-Hamed and S. Dimopoulos, JHEP **0506**, 073 (2005) [arXiv:hep-th/0405159].
 - [19] N. Arkani-Hamed, S. Dimopoulos, G.F. Giudice and A. Romanino, Nucl. Phys. **B709**, 3 (2005).
 - [20] G.F. Giudice and A. Romanino, Nucl. Phys. **B699**, 65 (2004).
 - [21] S. K. Gupta, P. Konar and B. Mukhopadhyaya, Phys. Lett. **B606**, 384 (2005) [arXiv:hep-ph/0408296].
 - [22] H. E. Haber and G. L. Kane, Phys. Rept. **117**, 75 (1985).
 - [23] See for example: V. S. Berezinskii *et al.*, *Astrophysics of Cosmic Rays*, Amsterdam: North-

Holland (1990).

- [24] A. Ibarra and D. Tran, JCAP JCAP **0807**, 002 (2008) [arXiv:0804.4596 [hep-ph]].
- [25] J. F. Navarro, C. S. Frenk and S. D. M. White, Astrophysics J. **462**, 563 (1996).
- [26] E. A. Baltz and J. Edsjo, Phys. Rev. D**59**, 023511 (1999) [arXiv:astro-ph/9808243].
- [27] I. Moskalenko and A. Strong, Astrophys. J.**493**, 694 (1998) [arXiv:astro-ph/9710124].
- [28] E. A. Baltz *et al.*, Phys. Rev. D**65**, 063511 (2002) [arXiv:astro-ph/0109318].